THE GERONTOLOGICAL SOCIETY OF AMERICA®

Journals of Gerontology: Biological Sciences
cite as: *J Gerontol A Biol Sci Med Sci*, 2016, Vol. 71, No. 2, 161–169
doi:10.1093/gerona/glv008
Advance Access publication March 3, 2015

OXFORD

Original Article

Senescence-Induced Oxidative Stress Causes Endothelial Dysfunction

Raj Bhayadia,[1,2] Bernhard M. W. Schmidt,[3] Anette Melk,[1,2,*] and Meike Hömme[1,2,*]

[1]Department of Pediatric Nephrology, Hepatology and Metabolic Diseases, Children's Hospital, Hannover Medical School, Hannover D-30625, Germany. [2]REBIRTH Excellence Cluster, Hannover Medical School, Hannover D-30625, Germany. [3]Department of Nephrology, Hannover Medical School, Hannover D-30625, Germany.

Address correspondence to Anette Melk, MD, PhD, Department of Pediatric Nephrology, Hepatology and Metabolic Diseases, Children's Hospital, Hannover Medical School, Carl-Neuberg-Strasse 1, D-30625 Hannover, Germany. Email: melk.anette@mh-hannover.de

*These authors contributed equally to this work.

Received June 11, 2014; Accepted January 16, 2015

Decision Editor: Rafael de Cabo, PhD

Abstract

Age is a risk factor for cardiovascular disease, suggesting a causal relationship between age-related changes and vascular damage. Endothelial dysfunction is an early pathophysiological hallmark in the development of cardiovascular disease. Senescence, the cellular equivalent of aging, was proposed to be involved in endothelial dysfunction, but functional data showing a causal relationship are missing.

Endothelium-dependent vasodilation was measured in aortic rings ex vivo. We investigated aortas from aged C57Bl/6 mice (24–28 months), in which $p16^{INK4a}$ and $p19^{ARF}$ expression, markers of stress-induced senescence, were significantly induced compared to young controls (4–6 months). To reflect telomere shortening in human aging, we investigated aortas from telomerase deficient ($Terc^{-/-}$) mice of generation 3 (G3). Endothelium-dependent vasodilation in aged wildtype and in $Terc^{-/-}$ G3 mice was impaired. A combination of the superoxide dismutase mimetic 1-Oxyl-2,2,6,6-tetramethyl-4-hydroxypiperidine (TEMPOL) and the nicotinamide adenine dinucleotide phosphate (NADPH) oxidase inhibitor apocynin significantly improved endothelium-dependent vasodilation in aged wildtype and $Terc^{-/-}$ G3 mice compared to untreated controls. We show that both, aging and senescence induced by telomere shortening, cause endothelial dysfunction that can be restored by antioxidants, indicating a role for oxidative stress. The observation that cellular senescence is a direct signalling event leading to endothelial dysfunction holds the potential to develop new targets for the prevention of cardiovascular disease.

Key Words: Biology of Aging—Cardiovascular Disease—Cellular Senescence—Endothelial—Mice

Cardiovascular disease is the most common cause of death in industrialized countries and its occurrence shows a strong correlation with advanced age. Age-associated changes are accelerated in cardiovascular disease (1) and reflect an increased risk for the progression of cardiovascular disease (2). However, age-associated changes occur in the absence of classical cardiovascular risk factors. The phenotype of the aged vasculature is characterized by functional changes and age-related atherosclerosis (3). Endothelial dysfunction is an important element of the changes occurring in the vasculature with age (4). One of the hallmarks of endothelial dysfunction is the inability of the endothelium to induce an appropriate vasodilatory response due to insufficient nitric oxide (NO) bioavailability (5). This endothelial-dependent vasodilation (EDD) can be measured and is an important research tool.

Cellular senescence is a phenotype of permanent and irreversible growth arrest and results in impaired cellular function and regeneration (6–8). It is associated with a distinct expression profile depending on the pathway used to reach senescence. Cells become senescent by telomere attrition, which induces p53 and in turn p53's main transactivational target $p21^{CIP1/WAF1}$ (9). Senescence that occurs independently of telomere shortening, for example via oxidative stress, leads to the induction of $p16^{INK4a}$ or $p19^{ARF}$ (10–12). Telomere shortening occurs with age in humans, mainly in arteries that are constantly under abrasive pressure and in need of active replenishment from replicated endothelial cells (13). Increased $p16^{INK4a}$ expression was found in atherosclerotic plaques from human vessels (14) and $p16^{INK4a}$ expression can be induced in cultured human endothelial cells (15). Cells from most mouse strains undergo senescence without

telomere shortening in presence of sustained telomerase expression, an enzyme inhibiting telomere attrition (16,17).

There is increasing evidence demonstrating that cellular senescence plays a role in the development of atherosclerosis (18–22). Endothelial dysfunction has been, however, only indirectly linked to cellular senescence. In cultured human aortic endothelial cells, the inhibition of telomere function induced the expression of intercellular adhesion molecule-1 and reduced endothelial NO synthase expression, features indicating dysfunction of endothelial cells (20). Although these findings raise the possibility that cellular senescence may be responsible for cardiovascular alterations, a direct functional link between the onset of cellular senescence and a decline in vascular function is missing.

Based on this observational data from cultured cells, we hypothesized that there is a causal relationship between the presence of senescence and endothelial dysfunction. In order to provide functional data, we investigated EDD in freshly isolated aortic rings from wildtype (WT) and telomerase deficient ($Terc^{-/-}$) mice. Since it had been shown for other cell types that senescence creates a microenvironment characterized by an increase in reactive oxygen species (ROS) (23–27), we also tested whether the senescence-mediated functional impairment of the endothelium was caused by the induction of oxidative stress.

Materials and Methods

Animals

Young (3–4-months old) and aged (24–28-months old) C57Bl/6 mice (referred to as young and aged wildtype, WT) were purchased from Janvier animal facility (Janvier SAS, St Berthevin Cedex, France). Heterozygote telomerase-deficient mice ($Terc^{+/-}$) mice on a C57Bl/6 background were purchased from Jackson Laboratories (Bar Harbor, ME) and bred as previously described (28). We observed significantly shorter telomeres (see Supplementary Figure 2) already in homozygote $Terc^{-/-}$ mice of the third generation (G3). We therefore used $Terc^{-/-}$ G3 mice (8–10-months old) and age-matched $Terc^{-/-}$ G1 and $Terc^{+/+}$ littermates for our experiments. All mice were housed in a day–night rhythm of 12 hours and had access to food and water ad libitum. To remove aortas and lungs, the animals were anesthetized using isoflurane (Baxter, Unterschleissheim, Germany) and euthanized thereafter. All procedures were performed in accordance with institutional guidelines for animal research and were approved by the local government authorities.

Isolation of Primary Endothelial Cells From Mouse Lungs

Primary endothelial cells were isolated from mouse lung tissue as described (29) with some modifications to allow for a sufficient cell quantity. Lungs were harvested and placed into ice-cold Hanks Balance Salt Solution (with Ca^{2+}/Mg^{2+}, Gibco, Life Technologies, Darmstadt, Germany). Lungs were cleared from connective tissue and then minced into smaller pieces. The tissue was transferred into Hanks Balance Salt Solution (without Ca^{2+}/Mg^{2+}, Gibco, Life Technologies), strained through a 40-µM mesh (BD Biosciences, Heidelberg, Germany), and digested with Dispase II (Roche, Mannheim, Germany) solution at 37°C for 1 hour. After homogenization the suspension was passed through 70-µM mesh (BD Biosciences) into DMEM/F-12 medium (Gibco, Life Technologies) supplemented with 10% fetal bovine serum (FBS, PromoCell, Heidelberg, Germany) to stop the digestion of the tissue suspension. The tissue suspension was mixed with Dynabeads (Invitrogen, Oslo, Norway) that were precoated with a secondary rat-anti-mouse CD144 antibody (BD Biosciences) and incubated for 30 minutes. Bound endothelial cells were collected by magnetic separation and resuspended in mouse endothelial medium (20% fetal bovine serum; endothelial cell medium, PromoCell). Endothelial cells from the lungs of two to four mice were pooled into one culture flask. Cells were allowed to grow for 3 days till confluence before first passage. First passage cells of mouse lung endothelial cells were used for the experiments.

Ex Vivo Aortic Ring Method

EDD and endothelium-independent vasodilation were determined ex vivo in isolated aortic rings using an FMI tissue organ bath (FMI; Föhr Medical Instrument, Seeheim, Germany). The descending thoracic aorta was carefully removed from the anesthetized animal and placed in cold (4°C) oxygenized Krebs–Henseleit physiological buffer (composition in mmol/L: NaCl 118; KCl 4.69; $CaCl_2$ 2.5; $MgSO_4$ 1.2; $NaHCO_3$ 25; KH_2PO_4 1.18; D-Glucose 5.6) at pH 7.4. The aortic vessel was carefully cleared of periadventitial fat under a preparation microscope (Stemi2000, Carl Zeiss, Göttingen, Germany) and cut transversely into 3–5-mm-long rings. The rings were mounted onto two parallel tungsten hooks in an organ bath chamber (IOA-5303, FMI) filled with Krebs–Henseleit buffer at 37°C. The isometric tension between the rings was measured by transducers (TMI-1020, 1030, FMI) and recorded on computer using software Bemon (FMI). All rings were equilibrated at a resting tension of 2.0 g for 1 hour. The muscular integrity and contractility of the rings were checked with repeated application of 50-mM KCl followed by washing with Krebs buffer till rings reach their resting tension.

EDD was measured by adding acetylcholine (ACh, Sigma-Aldrich, Steinheim, Germany) in increasing concentrations (10^{-9}–10^{-6} M) to previously preconstricted aortic rings. A stable preconstriction plateau was reached with phenylephrine (PE; Sigma-Aldrich) at 0.6 µM in young WT and $TERC^{-/-}$ mice and at 0.2 µM in aged WT mice, respectively. EDD was determined in all groups using ACh in presence or absence of NG-nitro-L-arginine methyl ester (L-NAME, Sigma-Aldrich; 10 µM, 30 minutes), superoxide dismutase mimetic 1-Oxyl-2,2,6,6-tetramethyl-4-hydroxypiperidine (TEMPOL; Sigma-Aldrich, 1 mM, 45 minutes) either alone or in combination with NADPH oxidase inhibitor apocynin (Sigma-Aldrich, 0.1 mM, 45 minutes). To study the effect of oxidative stress, aortic rings were incubated with L-buthionine-sulfoximine (BSO; Sigma-Aldrich, 1 mM, 90 minutes) followed by hydrogen peroxide (H_2O_2; Sigma-Aldrich, 1 µM, 30 minutes). Endothelium-independent responses for all groups were studied by providing glycerol nitrate (Nitrolingual infus, Phol Boskamp, Germany) in increasing concentrations (10^{-10}–10^{-5} M) as an external source of NO.

Telomere Length Measurement by Fluorescence In Situ Hybridization

Fluorescence in situ hybridization was performed on both nuclear preparations from isolated primary endothelial cells from mouse lungs and from paraffin sections of mouse aortas. To arrest cells in metaphase, isolated endothelial cells were treated with colcemid (Sigma-Aldrich, 10 ng/mL). Cells were harvested by trypsinization, resuspended in 75-mM KCl, and fixed in methanol/acetic acid

(3:1). Nuclear preparations were then spread on a glass slide and air-dried overnight before exposed to telomere probes. Paraffin sections of mouse aortas were deparaffinized, fixed in 4% formaldehyde (Carl-Roth, Karlsruhe, Germany) and enzymatically digested with pepsin (Sigma-Aldrich). After washing steps with phosphate buffered saline (Dulbecco PBS, Biochrom, Berlin, Germany) and a second fixation step in 4% formaldehyde, sections were dehydrated and air-dried.

Air-dried nuclear preparations and tissue sections were covered with hybridization mix containing a Cy3-conjugated, peptide nucleic acid (PNA) probe (Eurogentech, Seraing, Belgium) to detect telomeric sequences as previously described (28,30). Briefly, samples were denatured at 85°C for 3.5 minutes, followed by 2-hours incubation in a humidified chamber at 37°C in the dark. Slides were then washed twice with formamide-Tris-HCl buffer, pH 7.2, supplemented with 0.1% bovine serum albumin, and washed three times with TBS-T buffer (Tris-HCl, pH 7.2, 0.1% Tween). Sections were dehydrated, air-dried and mounted with mounting medium containing 4', 6-diamidino-2-phenylindole (DAPI; Carl-Roth) to counterstain nuclei. To avoid experimental variation and probe bleaching, we always probed a complete set of samples. Z-stacked images from stained nuclei were taken by fluorescence microscope (Axio observer Z1, Zeiss, Jena, Germany) with 100× objective. The mean telomere fluorescence intensity of each individual endothelial cell was analysed by Tfl-Telo V2 (Peter Lansdorp, Terry Fox Laboratory, British Columbia Research Centre, Vancouver, Canada). We included nuclei from cells arrested in metaphase and interphase in the analysis. Measurements were performed in at least 30 nuclei per sample. For cultured cells, we analysed a minimum of eight mice per group from two different experiments; for paraffin sections at least three mice per group were included.

Amplex Red Staining

A fluorometric-based horseradish peroxidase assay kit (Molecular probes, OR) was used to detect the production of hydrogen peroxide (31). Briefly, 3–4-mm freshly isolated aortic rings were carefully dissected on ice-cold modified Krebs-HEPES buffer (composition in mmol/L: NaCl 118; KCl 4; $CaCl_2$ 2.5; $MgSO_4$ 1.18; $NaHCO_3$ 24.9; KH_2PO_4 1.18; D-Glucose 11; EDTA 0.03; HEPES 20) under the preparation microscope, treated with chelex 100 (Sigma-Aldrich) 5 g/100 mL for 2 hour and adjusted to pH 7.4. The rings were longitudinally cut and opened to expose the endothelial layer followed by incubation with amplex red reagent (100 µM) and horseradish peroxidase (1 U/mL) at 37°C for 1 hour. Fluorescence was then measured with a microplate reader (Glomax multidetection system, Promega, CA) using excitation at 530 nm and fluorescence detection at 590 nm. Background fluorescence, determined as control without sample, was subtracted from each value.

Dihydroethidium Staining

Vascular superoxide levels were detected by dihydroethidium (DHE) staining on unfixed frozen sections as previously described (32,33). Freshly isolated aortas were carefully dissected in chelex-100–treated modified Krebs-HEPES buffer pH 7.4 and cleaned of connective tissue. Aortic segments were cut transversely and embedded in cyroembedding medium (Tissue Tek O.C.T. compound; Dako, CA), frozen in liquid nitrogen and stored at −80°C until used. 10-µm sections were brought to 37°C and equilibrated with prewarmed PBS to pH 7.4. Freshly prepared DHE (2 µM; Molecular probes) was applied and incubated for 30 minutes at 37°C protected from light. Control samples were similarly treated with PBS without DHE. After incubation, the vessels were gently washed with PBS. To study the effect of antioxidants, 0.1-mM apocynin and 1-mM TEMPOL were applied to slides for 45 minutes, prior to application of DHE. DHE is a lipophilic cell-permeable dye that is rapidly oxidized to ethidium in the presence of free radical superoxide, which can be detected using fluorescence microscopy. 3–4 entire visual fields of stained aortic tissues were captured with 200× maginification, and mean intensity of red-stained area was analyzed using ImageJ software (NIH, Bethesda, MD).

Immunohistochemistry and Immunofluorescence

Paraffin-embedded sections (3 µm) were deparaffinized and rehydrated. Antigen retrieval was performed at 125°C for 5 minutes in 10-mM citric acid buffer pH 6.0/0.05% Tween-20 using Dako pressure cooker (Dako). After incubation in blocking solution (5% nonfat milk prepared in PBS-0.05% Tween 20) for 1 hour, sections were incubated with anti-$p21^{CIP1/WAF1}$ antibody (1:250; Santacruz, TX) for 1 hr. After washing (PBS-0.05% Tween-20) the sections were incubated with for 30 minutes with a monoclonal anti-rabbit secondary antibody (Envision, Dako). Staining was visualized using Envision liquid DAB-substrate chromogen system (Dako).

For immunofluorescence studies involving vWF/γH2AX costaining, primary antibodies von Willebrand Factor (vWF) (1:350; Santacruz) and yH2AX (1:250, Millipore JBW301) were mixed in blocking solution and incubated overnight at 4°C. Cells were then incubated with a mix of secondary antibodies, anti-mouse alexa 555 (1:500; Life technologies, OR) and anti-rabbit alexa 488 (1:500; Life technologies), prepared in blocking solution for 1 hour. Nuclei were counterstained with 4,6-Diamidino-2-Phenylindole (DAPI). The images of endothelial cells were taken at 1,000× magnification. vWF- positive endothelial cells containing more than 4 γH2AX foci per nucleus were regarded as senescent. Costaining with Ki67 as previously described (8,34) was omitted in favor of vWF costaining as prior analysis using Ki67 immunohistochemistry in the respective sections had revealed the absence of proliferating endothelial cells.

$p67^{phox}$ Western Blot

Whole aortic tissue lysate was prepared in RIPA buffer (50-mM Tris-Cl pH 8.0, 150-mM NaCl, 1% NP-40, 0.5% deoxycholic acid, 0.1% SDS, 1-mM $NaVO_3$, 1-mM DTT, 1-mM phenylmethylsulfonyl fluoride) containing protease inhibitor tablets (Roche, Indianapolis, IN). Eighty to hundred micrograms of protein was loaded on 10% SDS polyacrylamide gels and were transferred to polyvinylidene difluoride membrane. The membrane was blocked with 5% milk in TBS-0.05% Tween-20 and incubated overnight at 4°C in anti-$p67^{phox}$ (1:1,000; Santacruz) diluted in blocking solution. Postincubation, the membrane was incubated in horseradish peroxidase–conjugated secondary anti-rabbit antibody (1:10,000) and the signal was visualized on x-ray films (Amersham, Buckinghamshire, UK) by exposing them to enhanced chemiluminescent horseradish peroxidase substrate (Amersham). The signals were normalized against housekeeping gene β-actin (Abcam, Cambrige, UK). Densitometric analysis of bands was performed by ImageJ.

Quantitative Real-Time Polymerase Chain Reaction (PCR)

Total RNA from total aortic tissues was isolated using RNeasy mini kit (Cat # 74104, Qiagen, Hilden, Germany). The RNA

was measured using Nanodrop photometer (PeQlab, Erlangen, Germany) at 260 and 280 nm to determine the concentration and purity of the sample. The samples were stored at −80°C until used. cDNA synthesis was carried out using Moloney murine leukemia virus reverse transcriptase (M-MLV RT, Life Technologies) and random hexamer primers (Life Technologies). For final reaction 1 µg of previously purified, high quality total RNA was used. After reverse transcription, real-time reaction was performed in an ABI7900 Real Time PCR cycler (Life Technologies) using the following intron-spanning primers and probes: $p16^{INK4a}$ forward 5′-GGG CAC TGC TGG AAG CC-3′, $p16^{INK4a}$ reverse 5′-AAC GTT GCC CAT CAT CAT C-3′, and $p16^{INK4a}$ probe 5′-CCG AAC TCT TTC GGT CGT A-3’; $p19^{ARF}$ forward 5′-TCG TGA ACA TCT TGT TGA GGC TA-3′, $p19^{ARF}$ reverse 5′-GTT GCC CAT CAT CAT CAT CAC CTG-3′, and $p19^{ARF}$ probe 5′-CGG TGC GGC CCT CTT CTC AAG ATC 3′; hypoxanthine phosphoribosyltransferase (HPRT) forward 5’-TGA CAC TGG TAA AAC AAT GCA AAC T-3′, HPRT reverse 5′- AAC AAA GTC TGG CCT GTA TCC AA-3′ and HPRT probe 5′-TCC ACC AGC AAG CTT GCA ACC TTA ACC-3′ were synthesized by Eurofins MWG Operon, (Ebersberg, Germany) and universal mastermix was purchased from Life Technologies. Specific gene expression was normalised against mouse HPRT gene as previously described (28).

Statistical Analysis

Data were evaluated using IBM SPSS 21. Means among treatment groups were compared using analysis of variance. Concentration-dependent vasodilation curves were analysed using the analysis of variance for repeated measurements. Data are given as means ± SEM.

Results

Aortas From Aged Mice Show Elevated Expression of Senescence Markers and show Rarefication of Endothelial Cells

We first addressed the question, whether there was an upregulation in senescence-associated gene expression in aortas from aged WT mice (24–28 months) when compared to young controls (4–6 months). In aortic lysates from aged animals, we detected increased $p16^{INK4a}$ and $p19^{ARF}$ mRNA expression (Figure 1A and B). On a single-cell level we found more $p21^{CIP1/WAF1}$-positive and γH2AX-positive endothelial cells (Figure 1C and D), along with a decreased number of endothelial cells (Figure 1E).

Endothelium-Dependent Dilation Is Reduced in Aged Mice

To investigate functional differences between young and aged mice, we tested their endothelium-dependent vasodilatory responses using an ex vivo aortic ring model. After preconstriction with phenylephrine, aortic rings were subjected to increasing ACh concentrations to measure their EDD. Aortic rings from aged mice showed a significantly decreased EDD compared with aortic rings from young mice (Figure 2A). To prove that this difference in vasodilation was really endothelium-dependent, we used glycerol nitrate as an external NO source. Aortic rings from aged mice dilated even better in presence of NO indicating that vascular smooth muscle cells are still functionally intact (Figure 2B). However, L-NAME, which blocks NO synthesis, nearly completely abolished EDD seen in aortic rings of both young and aged mice (Figure 2C).

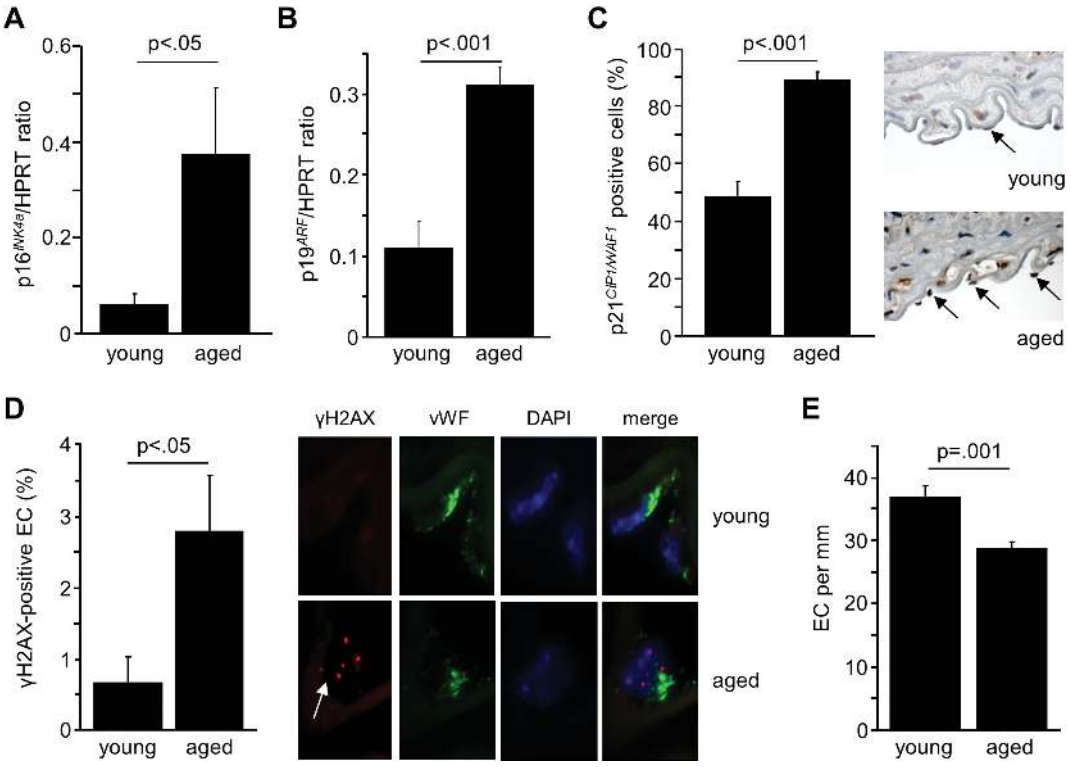

Figure 1. Expression of senescence markers in young and aged mice. (A) $p16^{INK4a}$ and (B) $p19^{ARF}$ mRNA expression in aortic tissue. (C) Number of $p21^{CIP1/WAF1}$ positive endothelial cells; representative staining. (D) γH2AX foci in endothelial cells from aortas of young and aged mice. Endothelial cells were identified by vWF expression, DAPI was used as a counterstain. (E) Number of endothelial cells lining the aortic vessel. Cells were counted in aortas stained for vWF, numbers are expressed per millimeter of aortic circumference.

Antioxidant Treatment Improves EDD in Aged Mice

We next investigated the impact of oxidative stress on the observed endothelial dysfunction in aged mice. ROS levels were increased in aortas from aged mice. We measured significantly elevated H_2O_2 concentrations, increased protein levels of the NADPH oxidase subunit $p67^{phox}$, and an increased O_2^- abundance in aged aortas (Figure 3A–C). To evaluate whether antioxidant treatment leads to an improvement of endothelial function, we incubated aortic rings from aged mice with a combination of the NADPH oxidase inhibitor apocynin and the superoxide dismutase mimetic TEMPOL. The combination of both antioxidants significantly lowered O_2^- abundance (Figure 3C) and improved EDD in aortic rings of aged mice (Figure 3D). This improvement was NO-dependent as treatment with L-NAME completely blocked EDD (Figure 3E). Treatment of aortic rings with TEMPOL or apocynin alone did not improve EDD in our model (data not shown).

To further support the role of oxidative stress for the impairment of EDD, we incubated aortic rings from aged mice with a noncytotoxic combination of BSO and H_2O_2. EDD was significantly reduced in BSO/H_2O_2-treated aortic rings as compared with untreated

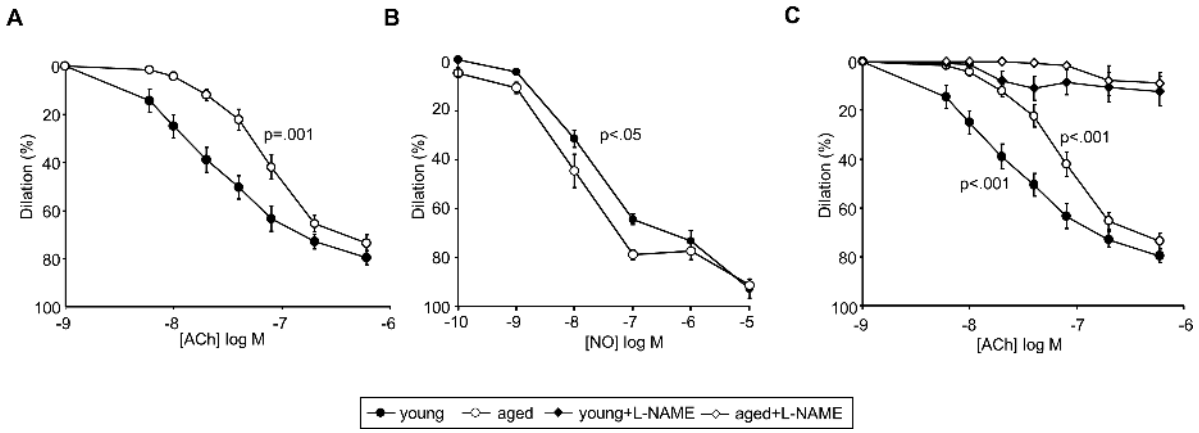

Figure 2. Effect of age on vasodilation. (A) Endothelium-dependent dilation (EDD) mediated by acetylcholine (ACh) in aortic rings from young ($n = 8$) and aged mice ($n = 15$). (B) Endothelium-independent dilation with glycerol nitrate as external source of nitric oxide (NO) (young: $n = 7$, aged: $n = 6$). (C) EDD in presence of L-NAME (young + L-NAME: $n = 8$, aged + L-NAME: $n = 4$); *p*-values indicate differences in presence/absence of L-NAME for the respective age group.

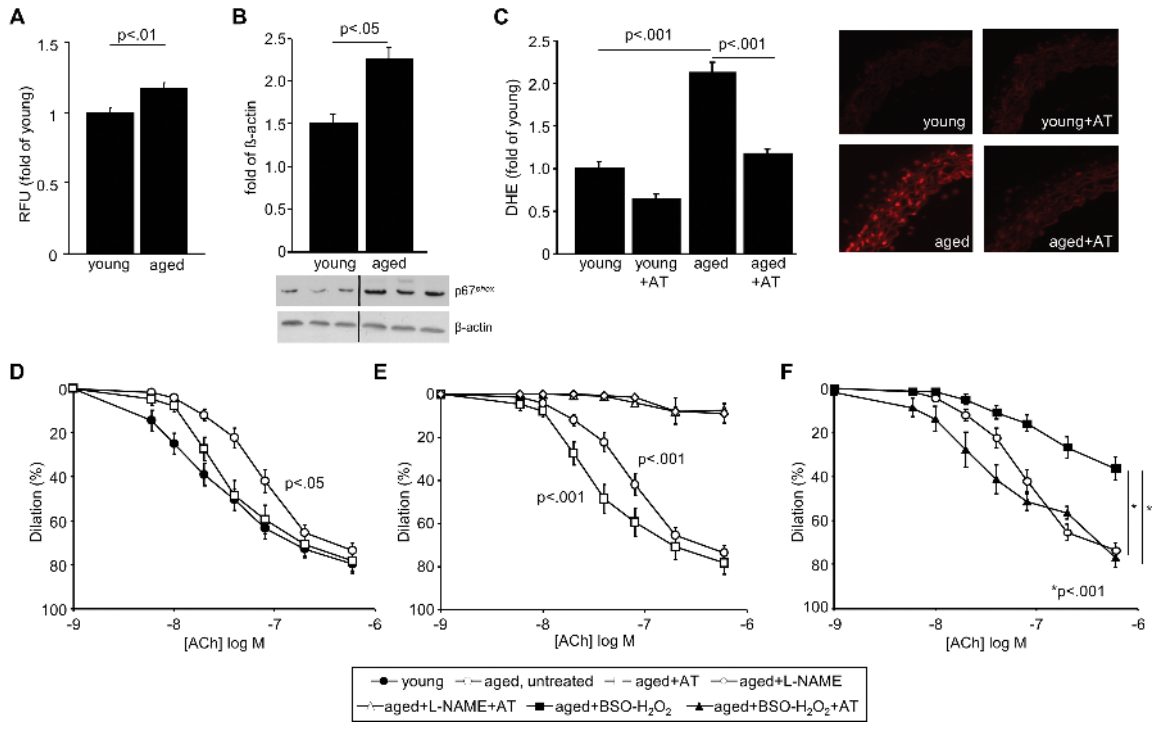

Figure 3. Antioxidants improve endothelium-dependent vasodilation (EDD) in aged mice. (A) H_2O_2 levels measured by Amplex Red fluorescence staining in aortic lysates. H_2O_2 levels are expressed as fold relative fluorescence units (RFU) of young aortas. (B) $p67^{phox}$ protein expression in relation to β-actin. (C) Dihydroethidium (DHE) staining in aorta sections from young and aged mice with/without preincubation of apocynin and TEMPOL (AT). (D) EDD in aortic rings from young and aged mice with/without preincubation of AT (aged + AT: $n = 8$). *p*-Value indicates the difference between AT-treated versus -untreated aortic rings from aged mice. (E) EDD in aortic rings from aged mice preincubated with/without AT in presence of L-NAME (aged + AT + L-NAME: $n = 6$). *p*-Values indicate difference between L-NAME-treated and -untreated groups with/without AT. (F) EDD in aortic rings from aged mice treated with BSO-H_2O_2 aortas with/without AT preincubation (BSO-H_2O_2: $n = 10$, BSO-H_2O_2 + AT: $n = 7$). *p*-Values indicate differences between BSO-H_2O_2 treated and untreated or BSO-H_2O_2 + AT-treated aortic rings, respectively.

controls (Figure 3F). Treatment with the combination of apocynin and TEMPOL was able to reverse the BSO/H_2O_2 treatment effect, and improved the vasodilatory response to a level comparable to aortic rings from young mice (Figure 3F).

Endothelial Cells From Terc$^{-/-}$ G3 Mice Display Short Telomeres and An Increase in Other Senescence Markers

Since WT mice possess long telomeres and express high telomerase activity, telomeres are maintained during aging (see Supplementary Figure 1). However, senescence through telomere shortening, as it occurs in human aging, can be studied in Terc$^{-/-}$ mice, which lack the RNA component of telomerase, and display significant telomere attrition at later generations, that is G3.

To confirm telomere shortening in endothelial cells of Terc$^{-/-}$ mice, telomere length was determined using telomere fluorescence in situ hybridization. Significantly shorter telomeres were present in the endothelial layer of aortas from of Terc$^{-/-}$ G3 and G4 in situ (Figure 4A; confirmation of the endothelial phenotype was done by vWF staining, see Supplementary Figure 2). This observation was confirmed in primary endothelial cells derived from lungs of Terc$^{-/-}$ G3 (Supplementary Figure 3). As expected, telomere length in endothelial cells from first generation Terc$^{-/-}$ (G1) mice was only slightly, and not significantly reduced compared to that of Terc$^{+/+}$ mice (Figure 4A and Supplementary Figure 2).

Along with the occurrence of shorter telomeres, we found an increase in p21$^{CIP1/WAF1}$-positive and γH2AX-positive endothelial cells in Terc$^{-/-}$ G3 aortas (Figure 4B and C). In addition, markers of stress-induced senescence, p16^{INK4a} and p19^{ARF}, were increased in aortic lysates of Terc$^{-/-}$ G3 mice (Figure 4D and E). Different to the situation in aged WT mice (Figure 1E), the total number of endothelial cells was not altered with higher generation (Supplementary Figure 4).

Endothelial Dysfunction in Presence of Critical Short Telomeres Is Rescued by Antioxidant Treatment

EDD of aortic rings from Terc$^{-/-}$G3 mice exposed to gradual increasing ACh concentrations was significantly reduced when compared to Terc$^{-/-}$ G1 and Terc$^{+/+}$ mice (Figure 5A). The vasodilatory response of aortic rings from Terc$^{-/-}$ G3 mice to glycerol nitrate as an external NO source was comparable to that of aortic rings from Terc$^{+/+}$ mice indicating a true impairment in endothelial function in Terc$^{-/-}$ G3 mice (Figure 5B). Treatment of aortic rings with the combination of antioxidants (apocynin and TEMPOL) significantly lowered O_2^- abundance in Terc$^{-/-}$ G3 mice (Figure 5C) and completely reversed the impairment in endothelial function (Figure 5D).

The increase in oxidative stress was confirmed by a greater amount of H_2O_2 in Terc$^{-/-}$ G3 aortas (Supplementary Figure 5A), whereas levels of the NADPH oxidase subunit p67^{phox} were not altered (Supplementary Figure 5B).

Comparing the vasodilatory response from Terc$^{-/-}$ G3 mice to that of aged mice, it is obvious that both show an impaired EDD. However, the dose-response curve toward increasing ACh doses in aged mice (Figure 3D) is shifted to the right. Instead Terc$^{-/-}$ G3 mice display a decrease in their maximum dilation capacity (Figure 5A). This difference is also highlighted in Supplementary Table 1 depicting maximum dilation and EC50 values.

Discussion

We show that the endothelial function is impaired in presence of aging and cellular senescence. Endothelial dysfunction was observed in both, aged WT and Terc$^{-/-}$ G3 mice, the later showing significantly shortened telomeres. Incubation with antioxidants was able to restore endothelial function suggesting a role for oxidative stress in age-related and senescence-mediated endothelial dysfunction. Our data suggest that cellular senescence is an important early

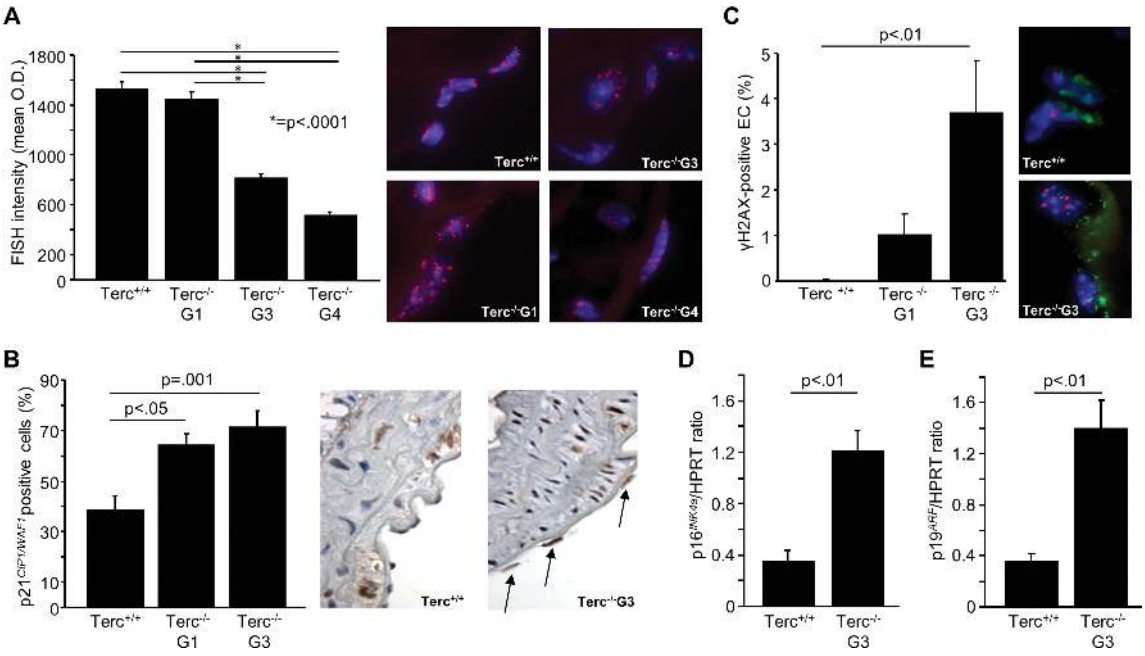

Figure 4. Effect of telomere shortening on the expression of other senescence markers. (A) Telomere length in endothelial cells of aortic rings from late generation Terc$^{-/-}$ mice (G3, G4) compared to G1 Terc$^{-/-}$ and Terc$^{+/+}$ mice; representative fluorescence in situ hybridization (FISH). (B) p21$^{CIP1/WAF1}$ positive endothelial cells; representative staining. (C) γH2AX-positive endothelial cells in aortas of Terc$^{+/+}$, Terc$^{-/-}$ G1, and Terc$^{-/-}$ G3 mice (D) p16^{INK4a} and (E) p19^{ARF} mRNA expression.

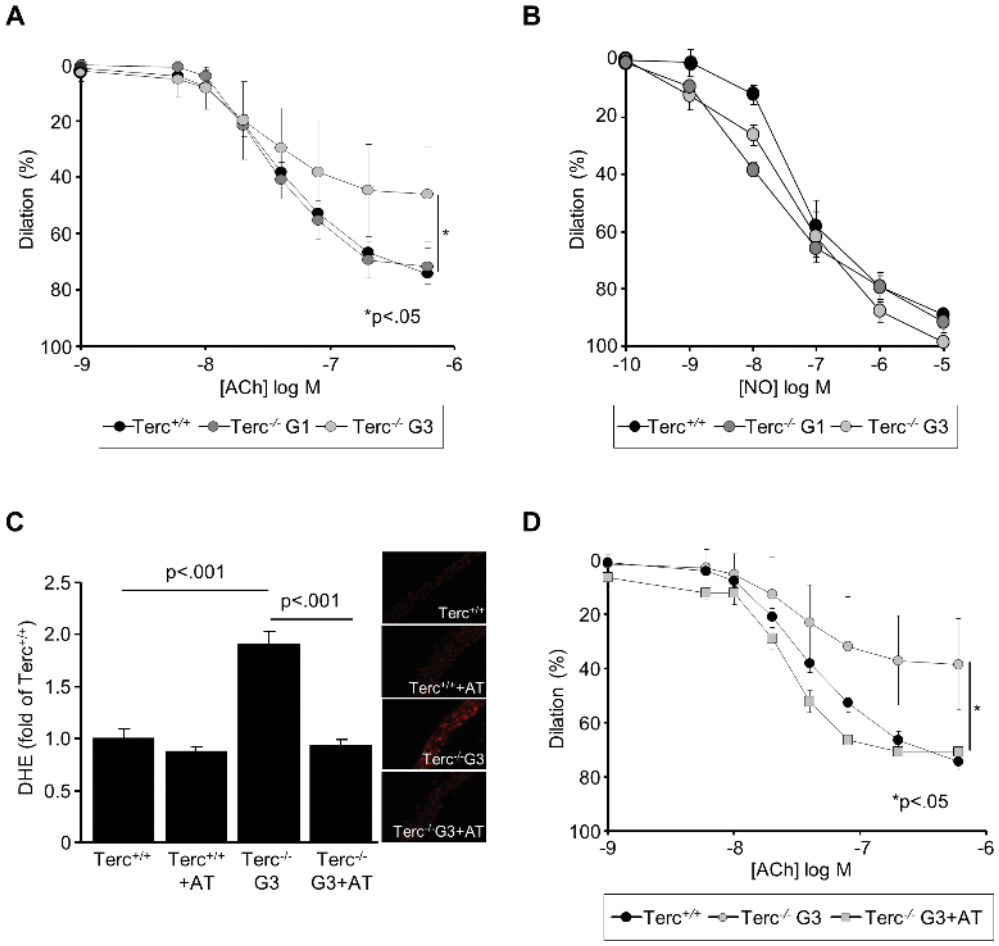

Figure 5. Effect of telomere attrition on ROS levels and vasodilation. (A) Endothelium-dependent vasodilation (EDD) in aortic rings from Terc$^{-/-}$ G3 mice ($n = 14$) compared to Terc$^{-/-}$ G1 ($n = 8$) and Terc$^{+/+}$ mice ($n = 17$). *p*-Value indicates the difference between Terc$^{-/-}$ G3 and Terc$^{+/+}$ mice. (B) Endothelial-independent dilation with glycerol nitrate as external nitric oxide (NO) source (Terc$^{-/-}$G3: $n = 6$, Terc$^{-/-}$G1: $n = 8$, Terc$^{+/+}$: $n = 8$). (C) EDD in aortic rings from Terc$^{-/-}$ G3 mice with or without preincubation of AT (Terc$^{-/-}$G3+AT: $n = 4$) compared to aortic rings from Terc$^{+/+}$ mice. *p*-Value indicates difference between AT-treated and -untreated Terc$^{-/-}$ G3 mice. (D) O_2^- levels, detected by DHE, in aortic rings from Terc$^{-/-}$ G3 mice with or without preincubation of apocynin and TEMPOL (AT).

mechanistic cornerstone of vascular degeneration that occurs as part of human aging.

We could demonstrate that there is a strong association between the presence of stress-induced cellular senescence and impaired endothelial function. Aged mouse aortas displayed an increased expression of senescence markers p16^{INK4a} and p19^{ARF}, proteins involved in stress-induced senescence (10,11). The increased number of p21$^{CIP1/WAF1}$-positive endothelial cells in aged aortas is in line with previous observations, which demonstrated that p21^{CIP1WAF1} was induced by oxidative stress in endothelial cells via ataxia telangiectasia mutated protein (35). In addition, we found an increase in DNA damage foci containing activated H2AX (γH2AX) in endothelial cells, which is regarded as a reliable indicator of senescence (8,36). Activation of a DNA damage response either at uncapped telomeres or at persistent DNA strand breaks especially in telomeric regions due to exogenous stressors is considered a major trigger for cell senescence (37–39). Similar to what has been shown in older human subjects (4), aged mouse aortas showed a significant reduction in EDD. We thereby extend previous findings of impaired EDD in older mice and rats (40–42) by connecting this functional decline to the presence of senescent endothelial cells. As demonstrated by the reduction in L-NAME-sensitive EDD, endothelial dysfunction in aged mice can be explained by the increase in ROS, and, as a consequence, reduced NO bioavailability.

We demonstrate a causal relationship between telomere shortening that also occurs in human aging and impaired endothelial function in Terc$^{-/-}$ mice. Aortic endothelial cells of late generation Terc$^{-/-}$ mice with short telomeres also displayed increased expression of other senescence markers. Short, dysfunctional telomeres via ataxia telangiectasia mutated signals lead to upregulation of p21$^{CIP1/WAF1}$ (43). The elevated ROS levels found in Terc$^{-/-}$ G3 mice might explain that also markers of stress-induced senescence increased and suggest a feedback-loop between telomere dysfunction, oxidative stress, and stress-induced senescence (44). Late-generation Terc$^{-/-}$ mice with critically short telomeres have been used to model for telomere attrition–dependent human aging (45–47). This mouse strain already served to study myocardial function (46,47) and decreased angiogenesis (48). Our focus has been on vascular physiology and we provide functional evidence for endothelial impairment in this mouse strain overcoming the limitations of pure cell culture studies (20). Aortic rings from Terc$^{-/-}$ G1 mice, which do not express the RNA component (Terc) of telomerase and still have long telomeres, showed no impairment in endothelial function. This observation ruled out the possibility that a loss of telomerase expression per se

or loss of previously reported telomere-independent, noncanonical functions of telomerase (49,50) result in endothelial dysfunction. In contrast to the model used by Poch and colleagues that found a protection from atherosclerosis in ApoE$^{-/-}$ mice with short telomeres (51) due to a already described reduction in the inflammatory response in presence of the immunosenescent phenotype of Terc$^{-/-}$ mice (52–55), our observations reflect a very early phase in the development of atherosclerosis, during which immunosenescence does not seem to be protective.

The incubation with antioxidants in aged WT and Terc$^{-/-}$ G3 mice restored vasodilatory function and highlights the functional link between the presence of senescence and oxidative stress. In fact, vasodilatory function is restored immediately with no need of longer incubation times as shown by others (56,57), but also without restoration of the senescence phenotype. Our results therefore confirm in vitro data showing that senescence is not only induced by, but also causes an increase in oxidative stress. Senescent cells activate downstream signalling pathways that trigger the production and release of ROS thereby creating a microenvironment characterized by increased oxidative stress (58). In human diploid fibroblasts, it has been shown that p16^{INK4a} expression causes increased ROS generation via PKCδ activation (27). Telomere attrition can cause ROS production by induction of p21$^{CIP1/WAF1}$ expression in human lung and mouse embryonic fibroblasts and in intestinal crypts of Terc$^{-/-}$ G4 mice (23). Passos and colleagues suggest a positive feedback loop between p21$^{CIP1/WAF1}$ and reactive oxygen production being necessary for the induction and maintenance of senescence (23).

Data derived from Terc$^{-/-}$ mice are instructive to better understand aging in humans and are thereby used to model human aging in our experimental design (45–47). It was therefore interesting to find differences between aortas from aged and Terc$^{-/-}$ G3 mice. Whereas aortas from aged mice needed higher ACh doses to reach dilatory responses similar to aortas from younger animals, Terc$^{-/-}$ G3 mice never reached the same vasodilatory response when compared to their respective counterparts. Together with our finding of less shedding of endothelial cells in Terc$^{-/-}$ G3 mice, one could speculate that the detected functional differences are due to a higher number of resident senescent endothelial cells in Terc$^{-/-}$ G3 mice creating a microenvironment that inhibits vasodilation.

In summary, we provide functional evidence that goes beyond available in vitro data showing endothelial impairment in the presence of senescent endothelial cells. Our results suggest that oxidative stress is the mediator of this senescence-induced endothelial dysfunction. Even though vascular aging is a complex process and it is difficult to reflect its complexity in model systems, we were able to identify cellular senescence pathways as important upstream signalling events for the development of endothelial dysfunction. This finding holds the potential of identifying new targets to prevent cardiovascular disease.

Funding

This work was supported by funding from the Deutsche Forschungsgemeinschaft (DFG, German Research Foundation) for the Cluster of Excellence REBIRTH (From Regenerative Biology to Reconstructive Therapy, EXC 62/3), and a DFG grant to A.M. (ME 3696/1-1). M.H. was supported by HILF (Hochschulinterne Leistungsförderung, Intramural grant of Hannover Medical School) and by the European Section of the Aldosterone Council (ESAC). R.B. participated in the Hannover Biomedical Research School (HBRS) Ph.D. program.

Acknowledgments

We would like to thank Dr. Christoph Jacobi for his helpful advice during the installation of the ex vivo aortic ring model. We are grateful to Julian Lünig, Esther Ermeling and Margit Überheide for their technical assistance.

References

1. Lakatta EG, Levy D. Arterial and cardiac aging: major shareholders in cardiovascular disease enterprises: Part II: the aging heart in health: links to heart disease. *Circulation*. 2003;107:346–354.
2. Laurent S. Defining vascular aging and cardiovascular risk. *J Hypertens*. 2012;30 Suppl:S3–S8.
3. Ungvari Z, Kaley G, de Cabo R, Sonntag WE, Csiszar A. Mechanisms of vascular aging: new perspectives. *J Gerontol A Biol Sci Med Sci*. 2010;65:1028–1041.
4. Donato AJ, Eskurza I, Silver AE, et al. Direct evidence of endothelial oxidative stress with aging in humans: relation to impaired endothelium-dependent dilation and upregulation of nuclear factor-kappaB. *Circ Res*. 2007;100:1659–1666.
5. Deanfield JE, Halcox JP, Rabelink TJ. Endothelial function and dysfunction: testing and clinical relevance. *Circulation*. 2007;115:1285–1295.
6. Hayflick LandMoorhead PS. The serial cultivation of human diploid cell strains. *Exp Cell Res*.1961;25:585–621.
7. Ben-Porath I, Weinberg RA. The signals and pathways activating cellular senescence. *Int J Biochem Cell Biol*. 2005;37:961–976.
8. Braun H, Schmidt BM, Raiss M, et al. Cellular senescence limits regenerative capacity and allograft survival. *J Am Soc Nephrol*. 2012;23:1467–1473.
9. Harley CB, Futcher AB, Greider CW. Telomeres shorten during ageing of human fibroblasts. *Nature*. 1990;345:458–460.
10. Serrano M, Lee H, Chin L, Cordon-Cardo C, Beach D, DePinho RA. Role of the INK4a locus in tumor suppression and cell mortality. *Cell*. 1996;85:27–37.
11. Wei W, Hemmer RM, Sedivy JM. Role of p14(ARF) in replicative and induced senescence of human fibroblasts. *Mol Cell Biol*. 2001;21:6748–6757.
12. Jacobi C, Hömme M, Melk A. Is cellular senescence important in pediatric kidney disease? *Pediatr Nephrol*. 2011;26:2121–2131.
13. Chang E, Harley CB. Telomere length and replicative aging in human vascular tissues. *Proc Natl Acad Sci U S A*. 1995;92:11190–11194.
14. Holdt LM, Sass K, Gäbel G, Bergert H, Thiery J, Teupser D. Expression of Chr9p21 genes CDKN2B (p15(INK4b)), CDKN2A (p16(INK4a), p14(ARF)) and MTAP in human atherosclerotic plaque. *Atherosclerosis*. 2011;214:264–270.
15. Chen J, Huang X, Halicka D, et al. Contribution of p16INK4a and p21CIP1 pathways to induction of premature senescence of human endothelial cells: permissive role of p53. *Am J Physiol Heart Circ Physiol*. 2006;290:H1575–H1586.
16. Wright WE, Shay JW. Telomere dynamics in cancer progression and prevention: fundamental differences in human and mouse telomere biology. *Nat Med*. 2000;6:849–851.
17. Kim H, You S, Farris J, et al. Expression profiles of p53-, p16(INK4a)-, and telomere-regulating genes in replicative senescent primary human, mouse, and chicken fibroblast cells. *Exp Cell Res*. 2002;272:199–208.
18. Samani NJ, Boultby R, Butler R, Thompson JR, Goodall AH. Telomere shortening in atherosclerosis. *Lancet*. 2001;358:472–473.
19. Fenton M, Barker S, Kurz DJ, Erusalimsky JD. Cellular senescence after single and repeated balloon catheter denudations of rabbit carotid arteries. *Arterioscler Thromb Vasc Biol*. 2001;21:220–226.
20. Minamino T, Miyauchi H, Yoshida T, Ishida Y, Yoshida H, Komuro I. Endothelial cell senescence in human atherosclerosis: role of telomere in endothelial dysfunction. *Circulation*. 2002;105:1541–1544.
21. Minamino T, Miyauchi H, Yoshida T, Tateno K, Kunieda T, Komuro I. Vascular cell senescence and vascular aging. *J Mol Cell Cardiol*. 2004;36:175–183.
22. Warboys CM, de LA, Amini N, et al. Disturbed flow promotes endothelial senescence via a p53-dependent pathway. *Arterioscler Thromb Vasc Biol*. 2014;34:985–995.

23. Passos JF, Nelson G, Wang C, et al. Feedback between p21 and reactive oxygen production is necessary for cell senescence. *Mol Syst Biol*. 2010;6:347.
24. Passos JF, Saretzki G, Ahmed S, et al. Mitochondrial dysfunction accounts for the stochastic heterogeneity in telomere-dependent senescence. *PLoS Biol*. 2007;5:e110.
25. Allen RG, Tresini M, Keogh BP, Doggett DL, Cristofalo VJ. Differences in electron transport potential, antioxidant defenses, and oxidant generation in young and senescent fetal lung fibroblasts (WI-38). *J Cell Physiol*. 1999;180:114–122.
26. Hutter E, Renner K, Pfister G, Stöckl P, Jansen-Dürr P, Gnaiger E. Senescence-associated changes in respiration and oxidative phosphorylation in primary human fibroblasts. *Biochem J*. 2004;380(Pt 3):919–928.
27. Takahashi A, Ohtani N, Yamakoshi K, et al. Mitogenic signalling and the p16INK4a-Rb pathway cooperate to enforce irreversible cellular senescence. *Nat Cell Biol*. 2006;8:1291–1297.
28. Westhoff JH, Schildhorn C, Jacobi C, et al. Telomere shortening reduces regenerative capacity after acute kidney injury. *J Am Soc Nephrol*. 2010;21:327–336.
29. Dong QG, Bernasconi S, Lostaglio S, et al. A general strategy for isolation of endothelial cells from murine tissues. Characterization of two endothelial cell lines from the murine lung and subcutaneous sponge implants. *Arterioscler Thromb Vasc Biol*. 1997;17:1599–1604.
30. Wang C, Maddick M, Miwa S, et al. Adult-onset, short-term dietary restriction reduces cell senescence in mice. *Aging (Albany NY)*. 2010;2:555–566.
31. Landmesser U, Dikalov S, Price SR, et al. Oxidation of tetrahydrobiopterin leads to uncoupling of endothelial cell nitric oxide synthase in hypertension. *J Clin Invest*. 2003;111:1201–1209.
32. Rey FE, Cifuentes ME, Kiarash A, Quinn MT, Pagano PJ. Novel competitive inhibitor of NAD(P)H oxidase assembly attenuates vascular O(2)(-) and systolic blood pressure in mice. *Circ Res*. 2001;89:408–414.
33. Csiszar A, Ungvari Z, Edwards JG, et al. Aging-induced phenotypic changes and oxidative stress impair coronary arteriolar function. *Circ Res*. 2002;90:1159–1166.
34. Berkenkamp B, Susnik N, Baisantry A, et al. In vivo and in vitro analysis of age-associated changes and somatic cellular senescence in renal epithelial cells. *PLoS One*. 2014;9:e88071.
35. Zhan H, Suzuki T, Aizawa K, Miyagawa K, Nagai R. Ataxia telangiectasia mutated (ATM)-mediated DNA damage response in oxidative stress-induced vascular endothelial cell senescence. *J Biol Chem*. 2010;285:29662–29670.
36. Lawless C, Wang C, Jurk D, Merz A, Zglinicki Tv, Passos JF. Quantitative assessment of markers for cell senescence. *Exp Gerontol*. 2010;45:772–778.
37. Wang C, Jurk D, Maddick M, Nelson G, Martin-Ruiz C, von Zglinicki T. DNA damage response and cellular senescence in tissues of aging mice. *Aging Cell*. 2009;8:311–323.
38. Fumagalli M, Rossiello F, Clerici M, et al. Telomeric DNA damage is irreparable and causes persistent DNA-damage-response activation. *Nat Cell Biol*. 2012;14:355–365.
39. Hewitt G, Jurk D, Marques FD, et al. Telomeres are favoured targets of a persistent DNA damage response in ageing and stress-induced senescence. *Nat Commun*. 2012;3:708.
40. Prévost G, Bulckaen H, Gaxatte C, et al. Structural modifications in the arterial wall during physiological aging and as a result of diabetes mellitus in a mouse model: are the changes comparable? *Diabetes Metab*. 2011;37:106–111.
41. Takenouchi Y, Kobayashi T, Matsumoto T, Kamata K. Gender differences in age-related endothelial function in the murine aorta. *Atherosclerosis*. 2009;206:397–404.
42. Wenzel P, Schuhmacher S, Kienhöfer J, et al. Manganese superoxide dismutase and aldehyde dehydrogenase deficiency increase mitochondrial oxidative stress and aggravate age-dependent vascular dysfunction. *Cardiovasc Res*. 2008;80:280–289.
43. Choudhury AR, Ju Z, Djojosubroto MW, et al. Cdkn1a deletion improves stem cell function and lifespan of mice with dysfunctional telomeres without accelerating cancer formation. *Nat Genet*. 2007;39:99–105.
44. Jacobs J, Jandde LT. Significant role for p16INK4a in p53-independent telomere-directed senescence. *Curr Biol*.2004;14:2302–2308.
45. Rudolph KL, Chang S, Lee HW, et al. Longevity, stress response, and cancer in aging telomerase-deficient mice. *Cell*. 1999;96:701–712.
46. Wong LS, Oeseburg H, de Boer RA, van Gilst WH, van Veldhuisen DJ, van der Harst P. Telomere biology in cardiovascular disease: the TERC-/- mouse as a model for heart failure and ageing. *Cardiovasc Res*. 2009;81:244–252.
47. Leri A, Franco S, Zacheo A, et al. Ablation of telomerase and telomere loss leads to cardiac dilatation and heart failure associated with p53 upregulation. *EMBO J*. 2003;22:131–139.
48. Franco S, Segura I, Riese HH, Blasco MA. Decreased B16F10 melanoma growth and impaired vascularization in telomerase-deficient mice with critically short telomeres. *Cancer Res*. 2002;62:552–559.
49. Ahmed S, Passos JF, Birket MJ, et al. Telomerase does not counteract telomere shortening but protects mitochondrial function under oxidative stress. *J Cell Sci*. 2008;121:1046–1053.
50. Haendeler J, Dröse S, Büchner N, et al. Mitochondrial telomerase reverse transcriptase binds to and protects mitochondrial DNA and function from damage. *Arterioscler Thromb Vasc Biol*. 2009;29:929–935.
51. Poch E, Carbonell P, Franco S, Díez-Juan A, Blasco MA, Andrés V. Short telomeres protect from diet-induced atherosclerosis in apolipoprotein E-null mice. *FASEB J*. 2004;18:418–420.
52. Herrera E, Martínez A, Blasco MA. Impaired germinal center reaction in mice with short telomeres. *EMBO J*. 2000;19:472–481.
53. Herrera E, Samper E, Martín-Caballero J, Flores JM, Lee HW, Blasco MA. Disease states associated with telomerase deficiency appear earlier in mice with short telomeres. *EMBO J*. 1999;18:2950–2960.
54. Lee HW, Blasco MA, Gottlieb GJ, Horner JW 2nd, Greider CW, DePinho RA. Essential role of mouse telomerase in highly proliferative organs. *Nature*. 1998;392:569–574.
55. Blasco MA. Immunosenescence phenotypes in the telomerase knockout mouse. *Springer Semin Immunopathol*. 2002;24:75–85.
56. Rippe C, Lesniewski L, Connell M, LaRocca T, Donato A, Seals D. Short-term calorie restriction reverses vascular endothelial dysfunction in old mice by increasing nitric oxide and reducing oxidative stress. *Aging Cell*. 2010;9:304–312.
57. Sindler AL, Fleenor BS, Calvert JW, et al. Nitrite supplementation reverses vascular endothelial dysfunction and large elastic artery stiffness with aging. *Aging Cell*. 2011;10:429–437.
58. Unterluggauer H, Hampel B, Zwerschke W, Jansen-Dürr P. Senescence-associated cell death of human endothelial cells: the role of oxidative stress. *Exp Gerontol*. 2003;38:1149–1160.